Energy Proceedings
Vol 41, 2024
ISSN 2004-2965

Experimental Study of Concentrated Solar-driven Methane Dry Reforming for Fuel Production

Xiangyu Yan[1,2], Fan Jiao[2,3], Shuzhan Ye[2,3], Shiying Yang[2,3], Yibiao Long[2,3], Taixiu Liu[2,3], Qibin Liu[2,3*]

1 International Research Center for Renewable Energy & State Key Laboratory of Multiphase Flow in Power Engineering, Xi'an Jiaotong University, Xi'an, 710049, China

2 Institute of Engineering Thermophysics, Chinese Academy of Sciences, Beijing,100190, China

3 University of Chinese Academy of Sciences, Beijing, 100190, China

(*Corresponding Author: qibinliu@mail.etp.ac.cn)

ABSTRACT

Methane dry reforming is a promising method of converting CH_4 and CO_2 into valuable fuels. Conventional approaches require the combustion of methane to achieve high reaction temperatures, resulting in energy wastage. This study investigates the use of concentrated solar energy as an alternative driving source for methane dry reforming to achieve the dual goals of increasing fuel production and saving energy. To this end, we design and optimize a solar reactor featuring the synthesis, molding, and characterization of Ni/CeO_2 catalysts. The performance of the methane dry reforming reaction is evaluated under different flow rates. The experimental results demonstrate that solar energy can be converted into fuel steadily for 8 hours with a solar-to-fuel efficiency of 13.98% when the catalyst is modeled to particle shape. This research makes a significant contribution to the development of eco-friendly and sustainable technologies for fuel production, offers application perspectives for a variety of industrial processes, and facilitates the integration of renewable energy sources.

Keywords: methane dry reforming, concentrated solar, solar reactor, Ni/CeO_2 catalyst

NONMENCLATURE

Abbreviations	
DRM	Dry reforming of methane
RWGS	Reverse water-gas shift
Symbols	
ΔG	Gibbs free energy change
F	Flow rate of gas
Y	Proportion of a gas in the total gas
X_i	Conversion rate of CH_4 or CO_2
η	Solar-to-fuel efficiency
r_{H_2}	Molar production rate of H_2
r_{CO}	Molar production rate of CO
r_{CH_4}	Molar reaction rate of CH4
$\Delta_c H^0$	Standard heat of combustion (298.15K) of H_2, CO, or CH_4
P	Power of light irradiation

1. INTRODUCTION

The rapid growth of energy demand makes it difficult for traditional fossil fuels to meet the energy requirements in the future [1]. The development and utilization of renewable energy have emerged as a crucial solution [2]. Among various renewable energy options, solar energy, which is both abundant and widely distributed, has obtained increasing attention [3]. The utilization of solar energy in the methane reforming process for clean fuel production demonstrates significant potential for efficient energy utilization [4]. Three frequently investigated methods for methane reforming include steam reforming of methane [5], dry reforming of methane (DRM) [6], and partial oxidation of methane [7]. Due to its highly endothermic nature and the ability to convert two greenhouse gases (CH_4 and CO_2), the DRM reaction has the greatest potential for clean solar fuel production [8]. This makes DRM the most

This is a paper for 15th International Conference on Applied Energy (ICAE2023), Dec. 3-7, 2023, Doha, Qatar.

promising approach for producing clean solar fuels from methane.

Many experimental studies have been conducted to evaluate the performance of concentrated solar-driven DRM. In 1991, the German Aerospace Research Establishment (DLR) carried out a concentrated solar-driven DRM, with air as a heat storage medium. The reaction temperatures can reach 1100 - 1500 °C, with conversion rates of approximately 70% for both CH_4 and CO_2 [9]. Steinfeld et al. [10] designed a fluid-wall aerosol flow reactor powered by concentrated solar energy, achieving conversion rates of 70% for CH_4 and 65% for CO_2 without the use of additional catalysts. This innovation addressed the issue of carbon deposition, which could otherwise negatively impact catalyst activity. In 1998, a study [11] investigated solar-driven volumetric receiver/reactor DRM, employing a ceramic foam structure based on α-Al_2O_3 and SiC ceramics as the absorber system, with γ-Al_2O_3 as the support material and Rh as the active metal. The CH_4 conversion rate exceeded 80%, and the power absorbed by the reactor ranged between 200 and 300 kW. While noble metal catalysts exhibited superior catalytic performance and stability, their high cost makes them less suitable for large-scale applications. In contrast, Ni-based catalysts, with the lower cost and high catalytic activity, emerge as more promising options for industrial use.

In this study, a volumetric receiver/reactor is designed for concentrated solar-driven DRM to produce solar fuels. The Ni/CeO_2 catalyst is synthesized and modeled into a particle shape. The influences of flow rates on CH_4 and CO_2 conversion rates and solar-to-fuel efficiency are investigated. These findings serve as a valuable reference for larger-scale productions of clean fuel through the DRM reaction driven by concentrated solar energy.

2. EXPERIMENT

2.1 Catalyst preparation

The preparation process of the Ni/CeO_2 catalyst is shown in Fig. 1. The CeO_2 support is prepared by calcining cerium nitrate hydrate ($Ce(NO_3)_3{\cdot}6H_2O$) at 500 °C for 3 hours. The introduction of Ni onto the CeO2 support is carried out by incipient wetness impregnation, using nickel nitrate hexahydrate ($Ni(NO_3)_2{\cdot}6H_2O$) as the precursor. Typically, 1.01 g of nickel precursor is dissolved in 1.20 mL of distilled water under stirring. After that, 1.80 g of as-prepared CeO_2 is added to the solution and stirred for 30 minutes. After aging for 12 hours at room temperature, the sample is dried at 110 °C for another 12 hours. The dried sample is decomposed by thermal calcination at 500 °C for 3 hours under static air. The obtained samples are denoted as NiO/CeO_2 powder, and subsequently molded into NiO/CeO_2 particles. Prior to the reaction, the molded samples require reduction through the flow of hydrogen. The resultant reduced catalyst is recognized as Ni/CeO_2 particle catalyst.

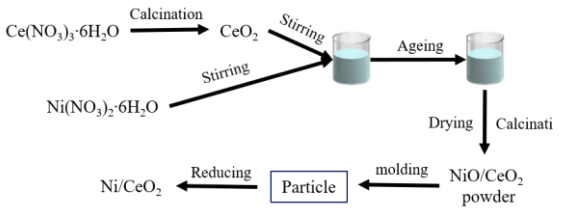

Fig. 1 The preparation process of the Ni/CeO_2 catalyst

2.2 Experimental equipment

The schematic diagram of the solar receiver/reactor is shown in Fig. 2.

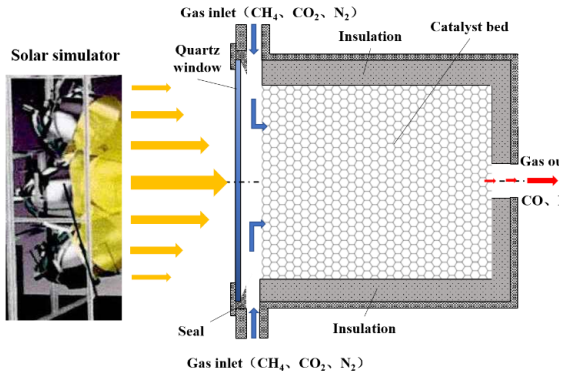

Fig. 2 Schematic diagram of the receiver/reactor

Concentrated solar energy is derived from a solar simulator, with the current being adjustable to regulate light intensities as required. The concentrated solar irradiates the catalyst bed directly through a quartz window to increase the temperature of the entire receiver/reactor. An insulation layer surrounds the catalyst bed to minimize radiation losses, and three thermocouples are inserted inside the catalyst to obtain temperatures at each location. The mass flow rates of CH_4, CO_2, N_2, and H_2 are controlled by mass flowmeters. Prior to the reaction, H_2 is mixed with N_2 to facilitate the reduction of NiO/CeO_2 to Ni/CeO_2 catalyst for 3 hours. After the reduction process, the catalyst bed is purged by pure N_2 for 1 hour to eliminate the H_2 from the receiver/reactor. A gas stream of CH_4, CO_2, and N_2 is fed to the receiver/reactor and contacts the catalyst to initiate the DRM reaction. The production gas is collected

and subsequently analyzed using a gas chromatograph. N_2 serves as an internal standard gas within the gas chromatograph to determine the composition of the production gas because it does not participate in the reaction.

3. RESULTS *AND* DISCUSSION

3.1 Characterization of catalyst

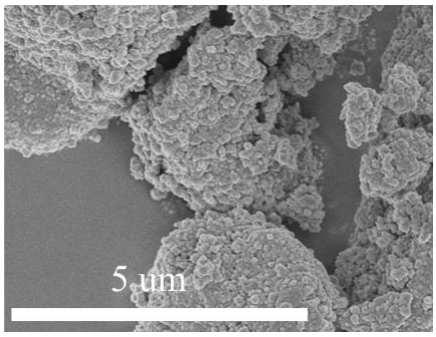

Fig. 3 SEM of the Ni/CeO_2 catalyst

The morphology and phase structure of the catalyst play a pivotal role in determining reaction performance. According to the SEM result in Fig. 3, the catalyst exhibits a composition of nanoparticles that aggregate at the micron scale. The SEM analysis conclusively validates the nanoscale structure of the catalyst.

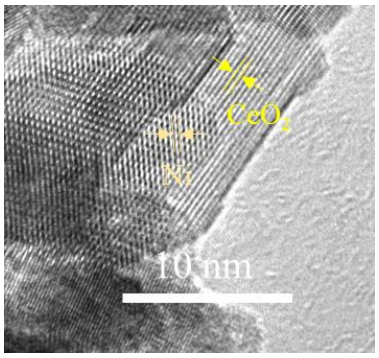

Fig. 4 TEM of the Ni/CeO_2 catalyst

The distribution of Ni and CeO_2 at the nanoscale holds significance for photo-thermal reactions. The TEM result in Fig. 4 illustrates that the Ni nanocrystals are in contact with CeO_2 nanocrystals directly. This interconnection between the two components is significant as it facilitates the separation of photo-generated carriers within the catalyst when exposed to solar irradiation. The TEM analysis provides additional confirmation that the catalyst exhibits a nanoscale structure.

3.2 Activity tests

3.2.1 Thermodynamic properties of the DRM reaction

The primary reactions that may occur in the process are listed in Eqs. (1) and (2). Eq. (1) is the target reaction, which consumes CH_4 and CO_2 to produce syngas. It has the highest enthalpy, so a high temperature is beneficial to the reaction. Eq. (2) is a reverse water-gas shift (RWGS) reaction, which is the main side reaction that consumes H_2 and increases the CO fraction in production.

$$CH_4 + CO_2 = 2CO + 2H_2 \qquad \Delta H^0_{298K} = 247\ \text{kJ/mol} \tag{1}$$

$$CO_2 + H_2 = H_2O + CO \qquad \Delta H^0_{298K} = 41\ \text{kJ/mol} \tag{2}$$

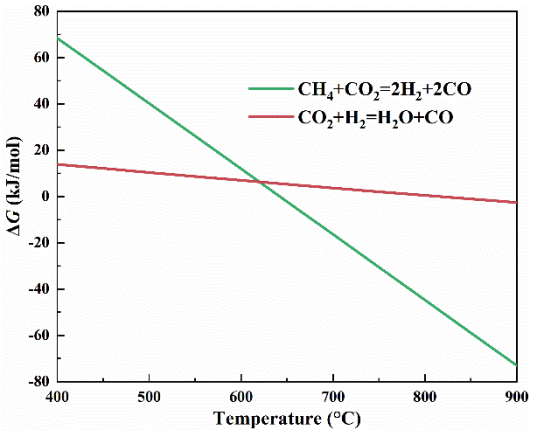

Fig. 5 Thermodynamic analysis of the Gibbs free energy change varying with temperatures

The standard Gibbs free energy change (Δ*G*) of the two reactions is plotted in Fig. 5. The DRM reaction in Eq. (1) is endothermic as it has a high standard enthalpy and requires temperatures above 640 °C to make the reaction spontaneous (T > 640°C, Δ*G* < 0). The RWGS reaction in Eq. (2) is one of the side reactions, which is spontaneous when the temperature is higher than 815 °C. Δ*G* of the DRM reaction is less than the RWGS reaction when the temperature is higher than 620 °C, which means that a higher temperature is more beneficial to promote the DRM reaction.

3.2.2 The performance of the receiver/reactor

The conversion rates of CH_4 and CO_2, the production rates of H_2 and CO, and the solar-to-fuel efficiency are used to indicate the performances of the receiver/reactor, which are calculated by:

$$F_{out} = \frac{F_{in} Y_{in,N_2}}{Y_{out,N_2}} \tag{3}$$

$$X_i = \frac{F_{in} Y_{in,i} - F_{out} Y_{out,i}}{F_{in} Y_{in,i}} \tag{4}$$

$$F_{out,j} = F_{out} Y_{out,j} \tag{5}$$

$$\eta = \frac{r_{H_2}\Delta_c H^0_{H_2} + r_{CO}\Delta_c H^0_{CO} - r_{CH_4}\Delta_c H^0_{CH_4}}{P} \quad (6)$$

where F_{out} is the total flow rate of the produced gas; Y is the proportion of a specific gas within a mixture of gases; X is the conversion rate of CH_4 or CO_2; r_{H_2} and r_{CO} are molar production rate of H_2 and CO; r_{CH_4} is the reaction rate of CH_4; $\Delta_c H^0_{H_2}$, $\Delta_c H^0_{CO}$, and $\Delta_c H^0_{CH_4}$ are the standard heat of combustion (298.15K) of H_2, CO, and CH_4; *P* is the power of light irradiation, tested by an energy densitometer. The power varies with the currents of the solar simulator, and the relationship is shown in Fig. 6. The power input into the receiver/reactor increases almost linearly with the currents, and the power in Eq. (6) can be calculated based on the current of the solar simulator.

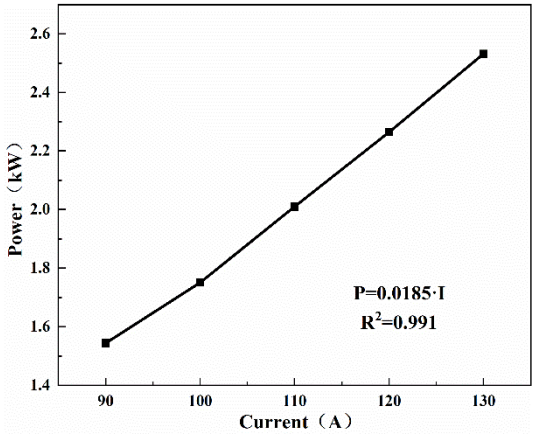

Fig. 6 The relationship between power and current

In the solar receiver/reactor, the temperature distribution is pivotal to elucidating the performance. Fig. 7 illustrates the temporal variation of the temperatures at the inlet, middle, and outlet of the receiver/reactor. Upon initiation of the solar simulator, the inlet temperature exhibits a rapid elevation due to its closest position to solar irradiation. Simultaneously, the temperatures at the middle and outlet exhibit gradual increments, attributable to the transfer of solar heat from the inlet toward these regions.

An obvious temperature change is observed upon the introduction of the reactants. As CH_4, CO_2, and N_2 flow through the catalyst bed, heat is conveyed from the inlet to the middle and outlet. Consequently, a temperature reduction at the inlet and temperature increases at the middle and outlet are detected. The temperature reduction at the inlet is also caused by the strong endothermic nature of the DRM reaction, which absorbs substantial heat, contributing to the decrease in temperature. Following 200 minutes of solar light irradiation, the temperatures nearly reach a steady state.

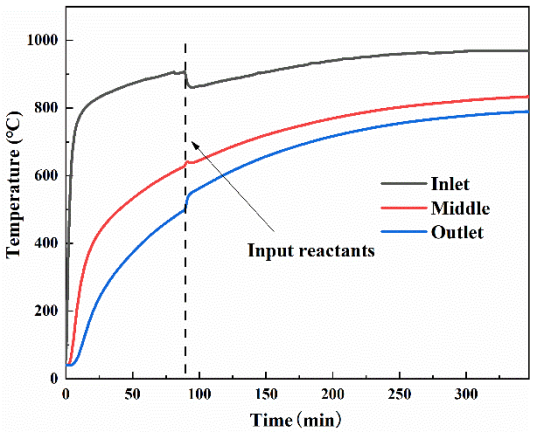

Fig. 7 The temperature change trends in the solar receiver/reactor

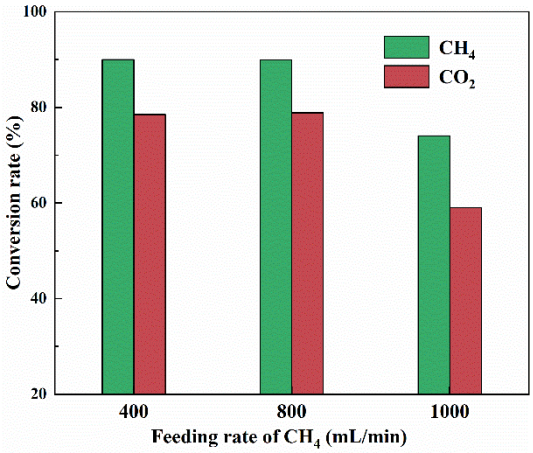

Fig. 8 The influences of reactants feeding rates on the conversion rates of CH_4 and CO_2

To inhibit the carbon formation from methane cracking reaction, the CO_2/CH_4 molar ratio is maintained at 1.5. The influences of reactant feeding rates on the conversion rates of CH_4 and CO_2 are shown in Fig. 8. The conversion rate of CH_4 is always higher than that of CO_2 due to the higher concentration of CO_2. As the feeding rates of reactants increase, both the conversion rates of CH_4 and CO_2 decrease, which is attributed to the higher space velocity. However, increasing feeding rates of reactants will increase the solar-to-fuel efficiency. Fig. 9 illustrates the effects of reactant feeding rates on solar-to-fuel efficiency and temperature. At the feeding rate of CH_4 is 1000mL/min, the solar-to-fuel is improved to 13.98%. Interestingly, the temperature decreases with the rising feeding rates of reactants due to the increase in heat carried away.

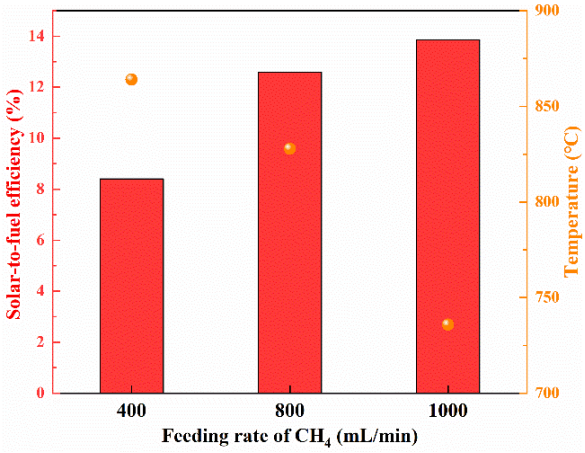

Fig. 9 The influences of feeding rates of reactants on the solar-to-fuel efficiency and temperature

4. CONCLUSIONS

In this work, a concentrated solar-driven dry reforming of methane fuel production system is established. A nanoscale Ni/CeO_2 catalyst is prepared by the method of incipient wetness impregnation and modeled into the particle shape. Comprehensive characterization of the catalyst through SEM and TEM reveals its morphology and phase structure. A thermodynamic analysis of the DRM reaction is conducted, and the advantageous conditions of higher temperatures are found. The evaluation indicators are outlined, and the relationship between the power input into the receiver/reactor and the current of the solar simulator is experimentally tested. This study explores the influences of reactant feeding rates on various performances, including CH_4 and CO_2 conversion rates and solar-to-fuel efficiency. A solar-to-fuel efficiency of 13.98% is obtained. These findings provide valuable insights for industrial DRM applications and the enhanced utilization of solar energy.

ACKNOWLEDGEMENT

The authors are grateful for the support provided by the National Key Research and Development Program of China (2021YFF0500701), the Major Program of the National Science Foundation of China (No. 52090061), and the National Science Fund for Distinguished Young Scholars (No. 52225601).

DECLARATION OF INTEREST STATEMENT

The authors declare that they have no known competing financial interests or personal relationships that could have appeared to influence the work reported in this paper. All authors read and approved the final manuscript.

REFERENCE

[1] Yao J-L, Zheng H-Y, Bai P-W, Liang W-P, Zhang Z-Y, Li T, et al. Design and optimization of solar-dish volumetric reactor for methane dry reforming process with three-dimensional optics-CFD method. Energy Conversion and Management. 2023;277.

[2] Lund H. Renewable energy strategies for sustainable development. energy. 2007;32:912-9.

[3] Fuqiang W, Qingzhi L, Huaizhi H, Jianyu T. Parabolic trough receiver with corrugated tube for improving heat transfer and thermal deformation characteristics. Applied energy. 2016;164:411-24.

[4] Jin J, Wei X, Liu M, Yu Y, Li W, Kong H, et al. A solar methane reforming reactor design with enhanced efficiency. Applied energy. 2018;226:797-807.

[5] Iulianelli A, Liguori S, Wilcox J, Basile A. Advances on methane steam reforming to produce hydrogen through membrane reactors technology: A review. Catalysis Reviews. 2016;58:1-35.

[6] Usman M, Daud WW, Abbas HF. Dry reforming of methane: Influence of process parameters—A review. Renewable and Sustainable Energy Reviews. 2015;45:710-44.

[7] Sengodan S, Lan R, Humphreys J, Du D, Xu W, Wang H, et al. Advances in reforming and partial oxidation of hydrocarbons for hydrogen production and fuel cell applications. Renewable and Sustainable Energy Reviews. 2018;82:761-80.

[8] Gao Y, Jiang J, Meng Y, Yan F, Aihemaiti A. A review of recent developments in hydrogen production via biogas dry reforming. Energy Conversion and Management. 2018;171:133-55.

[9] Buck R, Muir JF, Hogan RE. Carbon dioxide reforming of methane in a solar volumetric receiver/reactor: the CAESAR project. Solar Energy Materials. 1991;24:449-63.

[10] Dahl JK, Weimer AW, Lewandowski A, Bingham C, Bruetsch F, Steinfeld A. Dry Reforming of Methane Using a Solar-Thermal Aerosol Flow Reactor. Industrial & Engineering Chemistry Research. 2004;43:5489-95.

[11] Wörner A, Tamme R. CO2 reforming of methane in a solar driven volumetric receiver–reactor. Catalysis today. 1998;46:165-74.